ACS NANO

Article

Transparent, Flexible Silicon Nanostructured Wire Networks with Seamless Junctions for High Performance Photodetector Applications

Mozakkar Hossain, Gundam Sandeep Kumar, Barimar Prabhava S.N, Emmet D. Sheerin, David McCloskey, Somobrata Acharya, K. D.M. Rao, and John J Boland

ACS Nano, **Just Accepted Manuscript** • Publication Date (Web): 04 May 2018

ACS Publications

is published by the American Chemical Society. 1155 Sixteenth Street N.W., Washington, DC 20036

Transparent, Flexible Silicon Nanostructured Wire Networks with Seamless Junctions for High Performance Photodetector Applications

Mozakkar Hossain[⊥, ‡], Gundam Sandeep Kumar[‖, ‡], Barimar Prabhava S.N[#, ‡], Emmet D. Sheerin[#], David McCloskey[#], Somobrata Acharya[‖], K.D.M. Rao[⊥], and John J. Boland[#]*

[⊥]Technical Research Centre, Indian Association for the Cultivation of Science, Jadavpur, Kolkata-700032, India.

[#]School of Chemistry, Centre for Research on Adaptive Nanostructures and Nanodevices (CRANN), Trinity College Dublin, Dublin, Ireland.

[‖]Centre for Advanced Materials, Indian Association for the Cultivation of Science, Jadavpur, Kolkata-700032, India.

* To whom any correspondence should be addressed,

Email: trckdmr@iacs.res.in, mallik2arjun@gmail.com

[‡]These authors contributed equally to the paper

KEYWORDS: Transparent, Flexible, Silicon nanostructured wire network, Photodetector, Porous Silicon.

ABSTRACT: Optically transparent photodetectors are crucial in next generation optoelectronic applications including smart windows and transparent image sensors. Designing photodetectors with high transparency, photoresponsivity and robust mechanical flexibility remains a significant challenge, as is managing the inevitable tradeoff between high transparency and strong photoresponse. Here we report a scalable method to produce flexible crystalline Si nanostructured wire (NW) networks fabricated from silicon-on-insulator (SOI) with seamless junctions and highly responsive porous Si segments that combine to deliver exceptional performance. These networks show high transparency (~ 92% at 550 nm), broadband photodetection (350 nm to 950 nm) with excellent responsivity (25 A/W), optical response time (0.58 ms) and mechanical flexibility (1000 cycles). Temperature dependent photocurrent measurements indicate the presence of localized electronic states in the porous Si segments, which play a crucial role in light harvesting and photo-carrier generation. The scalable low-cost approach based on SOI has the potential to deliver new classes of flexible optoelectronic devices, including next generation photodetectors and solar cells.

Transparent electronics is a promising technology for producing devices that are transparent to visible light while delivering full device functionality,[1-3] and has the potential to impact a wide range of applications such as solar cells,[4] light emitting diodes,[5] and Li-ion batteries,[6] sensors[7] and photodetectors.[8] Transparent photodetectors, in particular, would enable new applications in smart windows, optical communications, video imaging, security and human motion detection.[9] The addition of flexibility further expands the range of applications to next generation optoelectronic devices[10] and holds the potential to meet the growing demands for light-weight compatibility, large-area scalability and adaptability to curved surfaces.[11]

Commercially available photodetectors are produced with crystalline silicon (Si), silicon carbide (SiC), InGaAs *etc*., which are rigid, brittle, expensive to fabricate and completely opaque.[12] Importantly, it is desirable to design transparent and flexible photodetectors with broad range spectral response that operate at room temperature.[13-14] The development of transparent photodetectors with excellent mechanical flexibility and high photoresponse over a broad spectral range remains a challenge.[10] Traditional thin-film based metal oxide transparent photodetectors have limited photoresponse and are constrained to rigid substrates.[15-20] Recently, there have been several attempts to fabricate transparent photodetectors using low-dimensional nanomaterials by exploiting their optical, electrical and mechanical properties.[2,8,9,21-27] Two-dimensional (2D) materials such as graphene[2], WSe_2[25] and WS_2[26] exhibit remarkably high photoresponse, but however, possess poor light absorption cross-sections and short carrier lifetimes. On the other hand, 1D nanowire (NW) based photodetectors have shown significant potential with high photosensitivity and ultra-fast response.[8-9, 21-24] Amongst the 1D materials studied to date, Si NWs have shown the most promise due to their well-controlled electrical and optical properties along with superior photoresponse performances.[14,28,29] High photoresponse from individual crystalline Si NW connected by short porous silicon segments has also been demonestrated.[30] Photoresponse of a single Si NW based photodetector was shown to increase with decreasing wire diameter.[31] However, devices based on individual NWs involve tedious lithography processes and limited to applications with small active areas.

Recently, percolative NW network based transparent photodetectors have received much attention.[8,9,21-24] Aligned SnO_2 NW based transparent photodetectors exhibited a good photoresponse but limited transparency.[9] Random percolative NW networks formed with SnO_2-ZnO showed good transparency but the photoresponse is restricted to a narrow spectral range.[23] Moreover, high contact resistance between individual NWs limits the photocurrent and response time of these devices.[8,9] To date, there has been no attempt to improve the contact resistance of these percolative NW networks. Here, we undertake the challenge of fabricating semiconducting NW networks with minimal contact resistance and high uniformity. We demonstrate the fabrication of transparent photodetectors using single-crystalline percolative Si NW networks with seamless junctions. The Si NW networks are successfully transferred onto a PET (polyethylene terephthalate) substrate to achieve 92% transparency at 550 nm. Photodetectors fabricated from these Si NW networks showed exceptional responsivity (25 A/W) over a wide spectral range from 350 nm to 950 nm, fast response times of 0.58 ms, in addition to excellent flexibility, making them suited for high performance transparent photodetector applications.

RESULTS AND DISCUSSION

The process for fabricating the Si NW network is based on crackle lithography in combination with Si dry etching (Figure 1). In the first step, acrylic resin nanoparticle dispersion is spin-coated on a silicon-on-insulator (SOI) substrate (Figure 1a) to produce the crackle template.[32] This is a simple, low-cost and scalable approach to forming uniform and highly interconnected nanostructured wire networks. In the second step, metal (Au/Ti) deposition and lift-off results in the formation of an Au NW network (see Figure 1b, c) that serves as an etch mask for patterning silicon in an inductive coupled plasma (ICP) etching process (see Figure 1d). The etching parameters are optimized to achieve Si NW network with flat edges over the entire 2 cm^2 area of the device. The patterned Si NW network is then transferred on to a PET substrate by etching the underlying SiO_2 layer of the SOI in HF solution (Figure 1e). In the final step, the metal over the Si NW network is etched to yield the Si NW network (Figure 1f). Randomly distributed localized regions of nanoporous Si are created within the crystalline Si NWs network using metal-assisted chemical etching (see Methods).[33] All the steps involved in this fabrication process are convenient, scalable and extensively used in the silicon industry.

The optical micrograph in Figure 1g shows the fabricated Si NWs are interconnected across the entire network with a uniform fill factor of 12%. The average width of a Si NW is

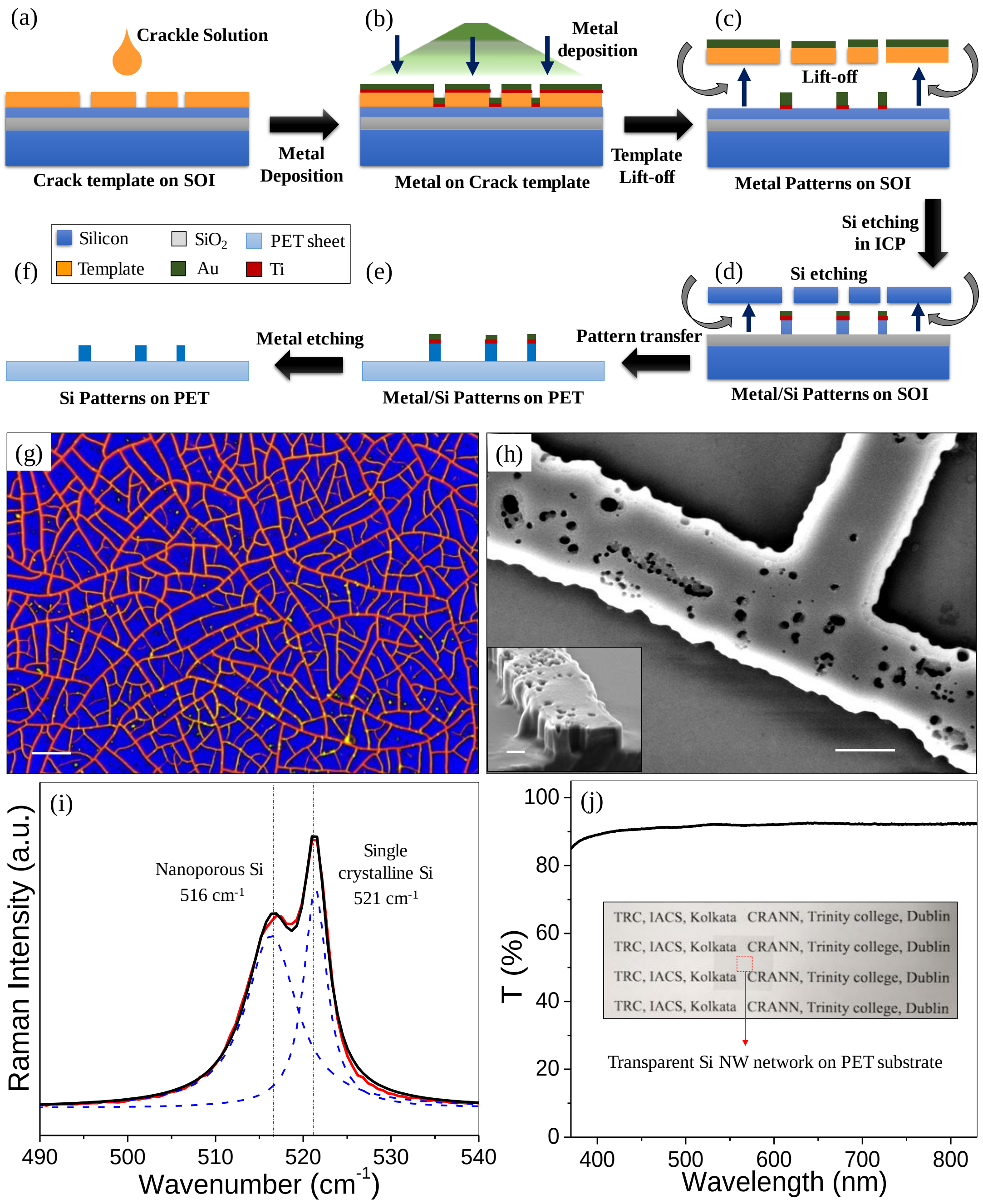

Figure 1. Schematic illustration of Si NW network fabrication (a) crackle template on SOI substrate, (b) deposition of the metal on template, (c) template lift-off, (d) after Si etching in ICP, (e) transferred to PET and (f) etching metals (Au, Ti), (g) Optical microscope image of a Si NW network on PET substrate (False color, scale bar 50 µm), (h) scanning electron microscope image of a Si NW network junction (600 nm scale bar) and inset shows cross sectional view of a Si NW (250 nm scale bar). (i) Raman spectra (red line) of Si NW network (blue dotted lines, black lines indicate deconvoluted peaks). (j) Transmittance spectrum of Si NW network, inset is a photograph of Si NW network on PET substrate.

870 ± 240 nm and average distance between the NWs is ~ 30 µm (Supporting Information, Figure S1). Scanning electron microscopy (SEM) images reveal the seamless junctions between Si NWs (Figure 1h) which are crucial for efficient carrier transport across the

network.[32] Cross sectional view of Si NW indicates the presence of steep edges (inset, Figure 1h). Interestingly, we observe the presence of nanopores with sizes ranging from 30 nm to 200 nm throughout the Si NW network (Supporting Information, Figure S2 and S3). The formation of the porous nanostructure is facilitated by using Au nanoparticles that are known to assist in chemical etching of Si susbtrates.[33] The porous nanostructure of Si NW network is crucial for achieving high performance photodetectors.[30] Raman spectrum of Si NW network shows peaks at 521 cm^{-1} and 516 cm^{-1} corresponding to single-crystalline Si and porous Si, respectively (Figure 1i).[34] TEM image of Si NW clearly demonstrates the porous nature, while the selected-area electron diffraction reveals the single-crystalline nature of the wires (Supporting Information, Figure S4). These observations demonstrate that the network is comprised of a random distribution of nanopores embedded within a Si single crystal framework. The transmission spectrum of the Si NW network shows uniform transmittance over the entire visible spectrum, displaying a transmittance of 92% at 550 nm (Figure 1j). This is higher than the expected transmittance based on the measured 12% fill factor, and attributed to the diffraction of light around the wire segments of Si NW network. Absorption of Si NW network in the UV region is found to increase gradually due to quantum confinement effects of the nanopores (Supporting Information, Figure S5).[35]

We have studied the performance of the Si NW network as a photodetector by depositing an array of Au electrodes using a shadow mask with 40 μm gap between electrodes (Supporting Information, Figure S6). The photoresponse characteristics of the device were measured with white light and monochromatic light of various wavelengths (800 nm, 700 nm, 600 nm and 500 nm). The current-voltage (I-V) characteristics indicate a pronounced photoresponse upon white light illumination in comparison to the dark current (Figure 2a). The photocurrent demonstrates a linear dependence with the illumination intensity and the device is not saturated in the intensity range used (Supporting Information, Figure S7).[36]

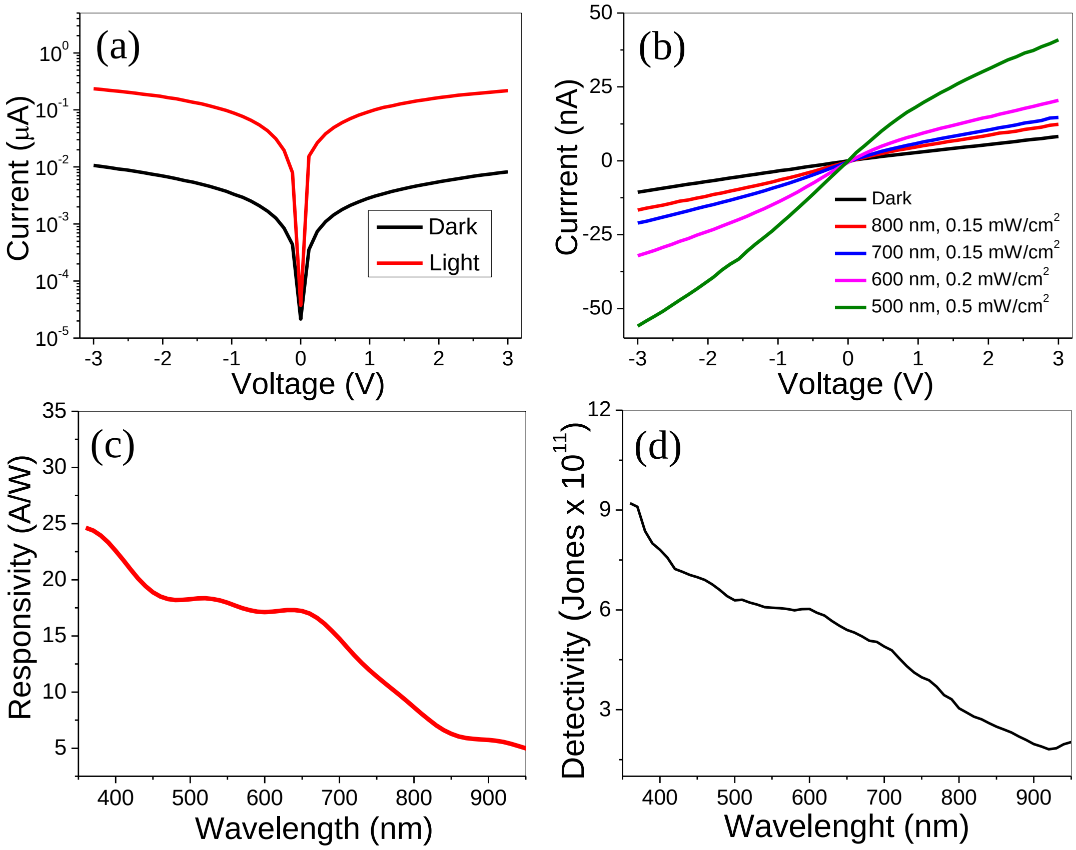

Figure 2. Current-voltage curves of Si NW network photodetector illuminated with, (a) white light (semi-logarithmic scale) of intensity 100 mW/cm^2, (b) monochromatic light of various wavelengths 500 nm, 600 nm, 700 nm and 800 nm and corresponding intensities are 0.5 mW/cm^2, 0.2 mW/cm^2, 0.15 mW/cm^2 and 0.15 mW/cm^2, respectively and in dark, (c) responsivity and (d) detectivity as a function of wavelength under an applied bias of 2 V.

A gradual increase in photocurrent is observed with decreasing wavelength from 800 nm to 500 nm (Figure 2b). The photosensitivity, which is defined as (I_{light}–I_{dark})/I_{dark}, is ~ 2000% under white light illumination of 100 mW/cm^2 for Si NW network with pores.[37] In contrast, a Si NW network without porosity shows a photosensitivity of ~ 300% (Supporting Information, Figure S8). The control experiment clearly demonstrates the importance of porosity in Si NW network for achieving high performance photodetectors, consistent with a previous report.[30] We have also tested traditional photodetector figure of merits such as responsivity and detectivity (Figure 2c,d).[13,38] The spectral responsivity R_λ is defined as $R_\lambda = J_{ph}/ P_{light}$, where $J_{ph} = I_{ph}/A$ is the photocurrent density; I_{ph}, P_{light} and A are the photocurrent, input light intensity and the effective area of the device respectively.[38,39] In our device, the effective area is considered to be 12% of total area of the device where the Si NW network is present. The spectral responsivity value is measured to be 24.6 - 4.9 A/W over the wavelength ranging from 350 nm to 950 nm (Figure 2c).

Another important parameter of a photodetector is detectivity, which is defined as $D = R_\lambda/(2qJ_d)^{1/2}$ (Supporting Information, Section 1) where R_λ is spectral responsivity, where q and J_d are the charge of the electron and dark current density, respectively.[29,39,40] The detectivity is found to be 9×10^{11} Jones (Figure 2d), which is comparable to commercially available Si-based non-transparent photodetectors (4×10^{12} Jones) and is higher than ZnO based transparent photodetectors.[41] The external quantum efficiency is measured to be 9000% (Supporting Information, Figure S9) for our transparent Si NW network photodetectors, which is comparable with other opaque photodetectors based on Mo-doped $ReSe_2$ nanosheets[42], MoO_3 nanosheets[43], and Nb_2O_5 nanoplates.[44] The device performance of Si NW network is notable compared to previously reported transparent detectors based on WSe_2[25], graphene[2], ZnO[41] and WO_3[16]. We have made a comprehensive survey of literature-reported on transparent photodetectors and compared the performances with our results (Supporting Information, table S1).[8,9,15-27] Our Si NW network photodetector exhibits the best spectral range, the maximum transparency and one of the best responsivity and detectivity values reported to date. The outstanding device performance is attributed to the porous Si structure and presence of seamless junctions across the Si NW network. As described below, the porous Si serves as a reservoir of charge carriers due to the presence of localized electronic states that release charge carriers under light illumination, whereas the seamless junctions ensure efficient transport of the carriers across the entire network due to the alignment of its bands relative to those in surrounding silicon.[45-47]

Response time is another important parameter for a photodetector which describes the ability of a device to switch in response to high speed optical signals. Transient photocurrent

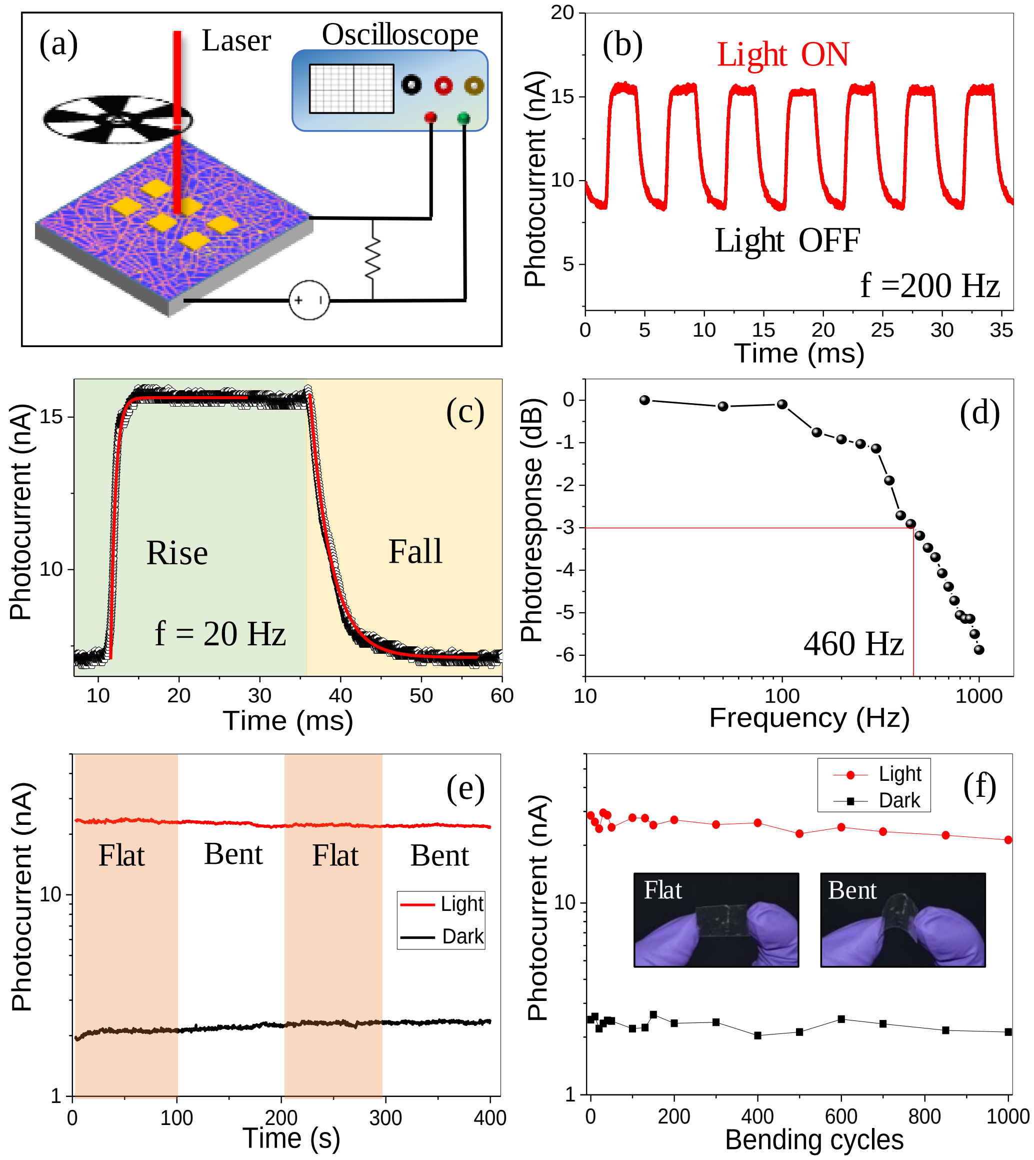

Figure 3. Transient photocurrent of the Si NW network at 650 nm light illumination under 2 V bias modulated by optical chopper with frequency, (a) schematic of the experimental setup, (b) transient photocurrent at 200 Hz and (c) rise time and fall time estimated at 20 Hz, black dots and red curves represent experimental data and exponential fits, respectively, (d) normalized photoresponse as a function of modulation signal frequency and corresponding cutoff frequency (f_{-3dB}) is 460 Hz, marked with red line. Time-dependent photocurrent plots for the flexible Si NW network photodetector (e) while it is in bent and flat positions, (f) the photocurrent and dark current after different bending cycles (1000). The inset shows the digital photographs of the device in flat and bent position.

measurements of Si NW networks were performed with red laser (laser power ~ 3 mW, 650 nm) to study the stability and repeatability of the photodetector using an optical chopper setup as shown in the Figure 3a. The transient photoresponse of the device under the dark and light illumination is measured by applying a bias of 2 V. Figure 3b illustrates the photocurrent of the Si NW network under modulated light of frequency 200 Hz. It is interesting to visualize the rapid increase and decrease in the photocurrent when the device is exposed to light (light ON) and dark (light OFF) respectively. The durability of the device was further tested by performing continuous ON/OFF switching for 1000 cycles at 500 Hz (Supporting Information, Figure S10c). The photocurrent characteristics reveal a stable, rapid photoresponse and reversible photo switching over multiple cycles. The photoresponse measurements at low frequency (20 Hz) as shown in Figure 3c, illustrate the saturation current in ON state and constant current in OFF state. Rise time and fall time are estimated using the following exponential equations, respectively (Supporting Information, Section 2).[48]

$$I = I_0 - I_0 \times e^{(-\frac{x}{t_r})} \quad \text{……………. (1)}$$

$$I = I_0 + A_1 \times e^{(-\frac{x}{t_f})} \quad \text{…………….. (2)}$$

For the representative single cycle shown in Figure 3c the rise and fall times are estimated to be 0.58 ms and 1.82 ms, respectively. This response time is the best reported value in literature for transparent photodetectors (Supporting Information, Table S1), which is attributed to the seamless junctions of NW in Si NW network. Figure 3d illustrates the normalized photoresponse as a function of modulation frequency from 20 Hz to 1 kHz for the Si NW network. The photoresponse is near constant in the low frequency region 20-100 Hz, consistent with the saturation of photocurrent (see Figure 3b, 3c and S10).[39,49] The frequency at which photoresponse becomes half of its initial value is called the cut-off frequency (f_{-3dB}), which is estimated to be 460 Hz.[38,39] These modulation frequency measurements indicate a faster performance compared to hybrid ZnO nanowire networks.[8,23] However our Si NW photodetector is slower than conventional silicon diodes, due to the carrier life time of trap states in the porous Si.

Flexibility and environment durability are crucial for practical applications of photodetectors.[10] The flexibility of the Si NW network photodetector was monitored by flexing the device up to a 5 mm bending diameter (Supporting Information, Figure S11). The photocurrent and dark current measured across the 40 μm device is shown in Figure 3e. The photoresponse remains unchanged in the flat and bent configurations, demonstrating the flexibility of the device. The minimal reduction in current on bending is attributed to the seamless junctions within the network and contrasts with the behavior in deposited NW networks where junction sliding is known to occur during deformation.[50] Figure 3f records the photocurrent and dark current of the device over the course of 1000 bending cycles. The photoresponse is effectively unchanged indicating excellent robustness, in addition to flexibility.

To investigate the mechanism of electrical transport through the Si NW network, we performed temperature dependent studies in dark as well as under illumination. Figure 4a shows the dark resistivity of Si NW network over the temperature range 100K to 325K, where the resistivity increases monotonically as the temperature is lowered. This behavior is consistent with 3D Mott variable range hopping (VRH) and the resistivity is well described by the following equation.[51]

$$\rho(T)= \rho_o(T) \exp[(T_o/T)^{1/4})] \text{ ....} (3)$$

where ρ is resistivity, T is temperature, ρ_o is characteristic resistivity and T_o is characteristic temperature. We estimate the density of states near Fermi energy to be $N(E_F) = 10^{19}$ $eV^{-1}.cm^{-3}$ using fitting parameters from equation 3 (Supporting Information, Section 3), which is comparable with polycrystalline Si.[46,52] 3D Mott VRH has previously been reported in vanadium oxide nanowire networks.[53] The enhanced DOS near Fermi energy ($N(E_F)$) indicates the existence of localized shallow trap states near the band edge.[52] The VRH model suggests that the conduction in porous Si NW network arises due to the hopping of charge carriers through localized trap states.[51] The photocurrent through Si NW network gradually increases with increasing intensity of light illumination (Figure 4b), although, the rate of increase of

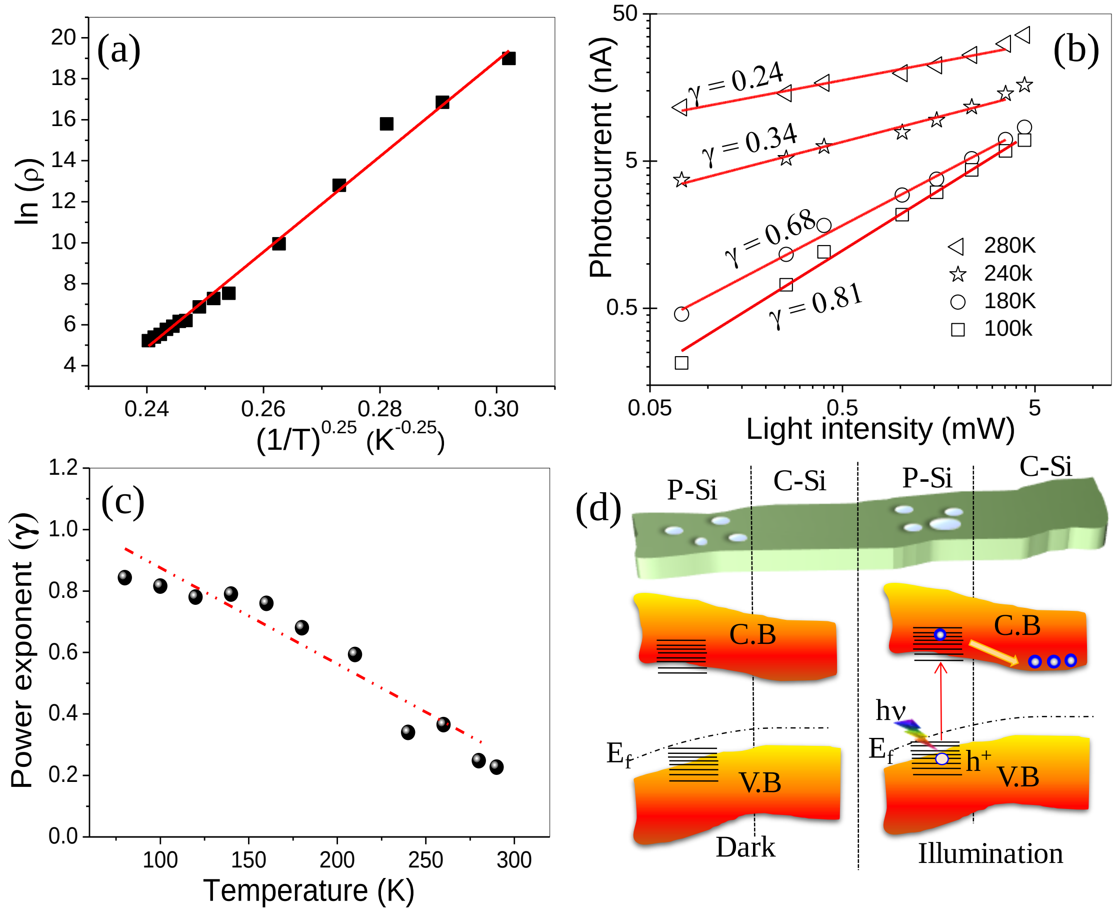

Figure 4. (a) Temperature dependence of resistivity with respect to $T^{-0.25}$ where T = 100K to 325K, red line is the linear fit for data. (b) Dependence of photocurrent with respect to white light intensity on the Si NW network under 2 V bias at various temperatures, red line is the power law fit ($I_{Ph} \propto P^{\gamma}$) for data. (c) Temperature dependence of power exponent γ under white light illumination. (d) Schematic representation of Si NWs with porosity, valence band and conduction band in dark and light illumination.

photocurrent is temperature dependent. The photocurrent (I_{ph}) scales with the light intensity (P) following a power law ($I_{ph} \propto P^{\gamma}$), where γ varies from 0.24 to 0.81 (Figure 4b).[54] This photoresponse is ascribed to induced photocurrent from extended trap states within the band gap of the porous Si.[55] The dependence on the light intensity approached the expected linear behavior at low temperature (at 100K, γ = 0.81) nevertheless it is sub-linear at high temperatures (at 280K, γ = 0.24). The change from a sub-linear to linear response is gradual (see Figure 4c), and consistent with electronic doping by localized trap states.[55] A similar photoresponse was observed in Si[31] and GaN[54] NWs.

Based on the above observations and performance of the device, we now speculate on the physical mechanism behind the photoresponse of our porous Si NW networks. Figure 4d depicts a schematic energy band diagram of the Si NW network with porous Si (P-Si) and crystalline Si (C-Si) segments in dark and under illumination. The band gap of P-Si is larger than that of C-Si due to the quantum confinement leading to enhanced absorption of UV light (Figure S5).[45] The surface defects of P-Si segments results in the formation of localized trap states as described in VRH model (Figure 4d).[51] In the dark, under applied bias the injected charge carriers are trapped in localized states, leading to low current. In contrast, the enhanced roughness of P-Si segments leads to reduced reflection and a stronger light interaction that allows charge carriers to be excited to the conduction band. The absorption of the UV light insures that charge carriers can be excited from broad range of localized trap states compared to lower energy visible-IR light, consistent with the high photoresponse in the UV region shown in Figure 2c.[30] The excited charge carriers from P-Si segments are swept into the C-Si segments due to their relative band alignment. The charge carriers can then easily reach the electrodes through neighbouring C-Si, facilitated by the seamless network junctions, resulting in the observed enhanced photoresponse and device performance.

Conclusions:

In summary, we have demonstrated the fabrication of Si NW networks with seamless junctions. The facile fabrication method results in the generation of localized P-Si regions while retaining the single-crystallinity of Si NW network, and was confirmed by SEM, TEM and Raman spectroscopy measurements. The Si NW network photodetector demonstrated a high transparency of 92% at 550 nm with an excellent response over a wide spectral range. Low-temperature and power law dependency measurements showed that the device performance originates from a reservoir of localized electronic states in the P-Si regions. Reliable and rapid photo switching characteristics with a response time of 0.58 ms was observed and attributed to the seamless nature of the junctions of Si NW network. Mechanical flexibility measurements showed the photoresponse performance was unaffected even after 1000 bending cycles. These devices are among the best performing transparent and flexible photodetectors ever reported. More importantly, the fabrication method developed here can be applied to thin films and 2D materials, with the potential to meet the demands of next generation optoelectronic devices.

Methods:

Fabrication of Si NW network: The commercially available SOI (silicon-on-insulator) with a 260 nm silicon (100) device layer with resistivity of 1-5 ohm.cm and 2 µm SiO_2 (SOITEC) wafers were used and patterned accordingly. The substrates are cleaned sequentially with water, acetone and isopropyl alcohol in ultrasonic bath for 10 minutes. Commercially available acrylic resin (Ming Ni Cosmetics Co., Guangzhou, China) solution was dispersed in water with a loading of ~ 0.2 to 2 mg/ml in deionized water. The dispersion was stirred for 10 minutes, and followed by ultrasonication for 30 minutes. The resultant dispersion was centrifuged at ~ 3000 rpm for 5 minutes to remove the large and un-dissolved particles of the acrylic resin. As prepared crackle solution was spin coated at 1000-2000 rpm for 2 minutes. Further, multi-layers of metals Ti (10 nm), and Au (50 nm to 100 nm) were sequentially deposited on the crackle template by thermal evaporation process (Hind High Vacuum Co., India). Sacrificial crackle templates were lifted off using the chloroform solution for 5-6 minutes. Inductive coupled plasma (ICP) etching process (OIPT Plasma Lab System100 ICP180, Oxford Instruments) with SF_6 and CHF_3 gases was employed to etch the exposed Si layer in between the metal wire network. In the next step, photoresist is patterned in the form of 50 µm holes separated by 100 µm pitch using optical lithography setup (OAL mask aligner). The photoresist patterns facilitate the transfer process from SOI substrate to PET sheet. The substrate with Si/Ti/Au NW network along with photo resist patterns was dipped in a diluted hydrofluoric

(HF) acid solution for 3 minutes to etch the SiO_2 (2 μm) layer. Subsequent dipping of substrate in water/ethanol (3:1) solution stimulates the Si NW network layer to float on top of the solution surface which is transferred onto a PET sheet (Supporting Information, Figure S12). The photoresist is removed in acetone and metal etching is performed for 1-5 minutes using Au etchant ($KI:I_2:H_2O$ in 2:1:5 ratio) and Ti etchant ($NH_4OH:H_2O_2$ in 1:2 ratio), respectively. The porous Si is obtained by dipping Si NW network in $HF:H_2O_2:H_2O$ (2:1:5 ratio) solution along with Au nanoparticles for 1-5 minutes (Supporting Information, Section 4).[33] The resultant PET substrates were annealed on hotplate at 80 ^oC for 5 minutes.

Fabrication of Si NW network based photodetectors: The substrates with Si NW network is dipped in 10% HF solution for 0.5 to 1 min to etch SiO_2 (surface oxide) on top of Si. Immediately, Au thin film electrodes were deposited using shadow mask with 40 μm gap electrodes. Before doing the electrical characterization, the devices were annealed at 80 ^oC for 10 min.

Photoconductivity measurements: The current–voltage characteristic measurements were carried out with the help of TTPx Lakeshore probe-station connected to a Keithley 4200 semiconductor characterization system (4200 SCS). The low temperature measurements were performed at ~ 10^{-5} mbar vacuum. For photoconductivity measurements, Newport Solar Simulator (model:66902) and Optem Schott light source were used. The wavelength dependent photocurrent measurements were performed using Newport Solar Simulator connected with monochromator. The frequency response measurements were conducted with a red laser diode (LD-RL-6-5v, ~ 3 mW, 650 nm), Thor labs optical chopper (MC2000B-EC) and oscilloscope (scientific instruments). The flexibility tests were performed using a home-built bending apparatus in tandem with probe station (Supporting Information, Figure S11).

Characterization techniques: Raman spectroscopy (Raman Triple spectrometer Jobin-Yvon T64000) measurements were carried out by exciting the sample with Nd:YAG green laser

(532.5 nm, ~ 2 mW power). Morphology of the silicon network was visualized using FESEM a Nova NanoSEM 600 instrument (FEI Co., The Netherlands). Transmission electron microscope (TEM) and selected area electron diffraction (SAED) patterns were measured using an ultrahigh resolution field emission gun transmission electron microscope (UHRFEG-TEM), JEOL, JEM 2100 F field emission electron microscope. Transmission measurements were performed using the Varian Cary 5000 UV-Vis-NIR spectrophotometer.

ASSOCIATED CONTENT

The supporting information is available free of charge on the ACS Publications website. Further information on the Si NW wire network fabricated in this study, including diameter and pore size distribution statistics, UV-Vis spectra, SEM, TEM and Optical microscopy imaging, external quantum efficiency. A comprehensive survey of literature on transparent photodetectors Table S1 is also included. The experimental details regarding Si NW network, including transferring on PET sheet, porosification process and flexibility measurement set-up. The authors declare no competing financial interest.

AUTHOR INFORMATION

Corresponding Author

** Email: trckdmr@iacs.res.in, mallik2arjun@gmail.com

Author Contribution

M.H., G.S.K., B.P.S. and K.D.M. designed and performed the experiments; E.D.S., and D.M., performed the transient photoresponse experiments; M.H., G.S.K. and B.P.S. analyzed the data. M.H., G.S.K., B.P.S., S.A., J.B. and K.D.M. wrote the manuscript; K.D.M. performed overall guidance of the project. All authors read and approved the manuscript. M.H., G.S.K. and B.P.S. contributed equally.

ACKNOWLEDGMENT

The authors are grateful to Prof. G. U. Kulkarni and Prof. Santanu Bhattacharya for their encouragement. This work was supported by Technical Research Centre (TRC, Project No. AI/1/62/IACS/2015), IACS, Kolkata, Science and Engineering Research Board (SERB, Project No. ECR/2017/003264, EMR/2014/000664), India and European Research Council under Advanced Grant 321160 and Science Foundation Ireland (SFI) under grant number 12/IA/1482. G.S.K. acknowledges DST INSPIRE Programme for fellowship. We thank Dr. Ravindra Pandey for useful discussions. We dedicate this manuscript to Prof. G. U. Kulkarni.

REFERENCES

(1) McCoul, D.; Hu, W.; Gao, M.; Mehta, V.; Pei, Q. Recent Advances in Stretchable and Transparent Electronic Materials. *Adv. Electron. Mater.* **2016,** *2*, 1500407.

(2) Liu, N.; Tian, H.; Schwartz, G.; Tok, J. B. H.; Ren, T. L.; Bao, Z. Large-Area, Transparent, and Flexible Infrared Photodetector Fabricated Using P-N Junctions Formed by N-Doping Chemical Vapor Deposition Grown Graphene. *Nano Lett.* **2014,** *14*, 3702-3708.

(3) Mativenga, M.; Geng, D.; Kim, B.; Jang, J. Fully Transparent and Rollable Electronics. *ACS Appl. Mater. Interfaces* **2015,** *7*, 1578-1585.

(4) Zhao, Y.; Meek, G. A.; Levine, B. G.; Lunt, R. R. Near-Infrared Harvesting Transparent Luminescent Solar Concentrators. *Adv. Optical Mater.* **2014,** *2*, 606-611.

(5) Gu, G.; Bulović, V.; Burrows, P. E.; Forrest, S. R.; Thompson, M. E. Transparent Organic Light Emitting Devices. *Appl. Phys. Lett.* **1996,** *68*, 2606-2608.

(6) Yang, Y.; Jeong, S.; Hu, L.; Wu, H.; Lee, S. W.; Cui, Y. Transparent Lithium-ion Batteries. *Proceed. of the National Acad. of Sci.* **2011,** *108*, 13013-13018.

(7) Lee, S.; Reuveny, A.; Reeder, J.; Lee, S.; Jin, H.; Liu, Q.; Yokota, T.; Sekitani, T.; Isoyama, T.; Abe, Y.; Suo, Z.; Someya, T. A Transparent Bending-Insensitive Pressure Sensor. *Nat. Nanotechnol.* **2016,** *11*, 472-478.

(8) Zheng, Z.; Gan, L.; Li, H.; Ma, Y.; Bando, Y.; Golberg, D.; Zhai, T. A Fully Transparent and Flexible Ultraviolet–Visible Photodetector Based on Controlled Electrospun ZnO-CdO Heterojunction Nanofiber Arrays. *Adv. Funct. Mater.* **2015,** *25*, 5885-5894.

(9) Huang, S.; Guo, C. F.; Zhang, X.; Pan, W.; Luo, X.; Zhao, C.; Gong, J.; Li, X.; Ren, Z. F.; Wu, H. Buckled Tin Oxide Nanobelt Webs as Highly Stretchable and Transparent Photosensors. *Small* **2015,** *11*, 5712-5718.

(10) Xie, C.; Yan, F. Flexible Photodetectors Based on Novel Functional Materials. *Small* **2017,** *13*, 1701822.

(11) Gupta, R.; Rao, K. D. M.; Kiruthika, S.; Kulkarni, G. U. Visibly Transparent Heaters. *ACS Appl. Mater. Interfaces* **2016,** *8*, 12559-12575.

(12) Saran, R.; Nordin, M. N.; Curry, R. J. Facile Fabrication of PbS Nanocrystal:C_{60} Fullerite Broadband Photodetectors with High Detectivity. *Adv. Funct. Mater.* **2013,** *23*, 4149-4155.

(13) Dhanabalan, S. C.; Ponraj, J. S.; Zhang, H.; Bao, Q. Present Perspectives of Broadband Photodetectors Based on Nanobelts, Nanoribbons, Nanosheets and the Emerging 2D Materials. *Nanoscale* **2016,** *8*, 6410-6434.
(14) Zou, H.; Li, X.; Peng, W.; Wu, W.; Yu, R.; Wu, C.; Ding, W.; Hu, F.; Liu, R.; Zi, Y.; Wang, Z. L. Piezo-phototronic Effect on Selective Electron or Hole Transport through Depletion Region of Vis–NIR Broadband Photodiode. *Adv. Mater.* **2017,** *29*, 1701412.
(15) Shin, S. W.; Lee, K.-H.; Park, J.-S.; Kang, S. J. Highly Transparent, Visible-Light Photodetector Based on Oxide Semiconductors and Quantum Dots. *ACS Appl. Mater. Interfaces* **2015,** *7*, 19666-19671.
(16) Qi, Z.; Cao, J.; Ding, L.; Wang, J. Transparent and Transferrable Organic Optoelectronic Devices Based on WO_3/Ag/WO_3 Electrodes. *Appl. Phys. Lett.* **2015,** *106*, 053304.
(17) Patel, M.; Kim, H.-S.; Kim, J. All Transparent Metal Oxide Ultraviolet Photodetector. *Adv. Electron. Mater.* **2015,** *1*, 1500232.
(18) Kim, H.-S.; Kumar, M. D.; Park, W.-H.; Patel, M.; Kim, J. Cu_4O_3-Based All Metal Oxides for Transparent Photodetectors. *Sensors and Actuators A: Physical* **2017,** *253*, 35-40.
(19) Zhang, H.; Jenatsch, S.; De Jonghe, J.; Nüesch, F.; Steim, R.; Véron, A. C.; Hany, R. Transparent Organic Photodetector Using a Near-Infrared Absorbing Cyanine Dye. *Sci. Rep.* **2015,** *5*, 9439.
(20) Kim, H.-S.; Chauhan, K. R.; Kim, J.; Choi, E. H. Flexible Vanadium Oxide Film for Broadband Transparent Photodetector. *Appl. Phys. Lett.* **2017,** *110*, 101907.
(21) Liu, X.; Liu, X.; Wang, J.; Liao, C.; Xiao, X.; Guo, S.; Jiang, C.; Fan, Z.; Wang, T.; Chen, X.; Lu, W.; Hu, W.; Liao, L. Transparent, High-Performance Thin-Film Transistors with an InGaZnO/Aligned-SnO_2-Nanowire Composite and their Application in Photodetectors. *Adv. Mater.* **2014,** *26*, 7399-7404.
(22) Liu, X.; Jiang, L.; Zou, X.; Xiao, X.; Guo, S.; Jiang, C.; Liu, X.; Fan, Z.; Hu, W.; Chen, X.; Lu, W.; Hu, W.; Liao, L. Scalable Integration of Indium Zinc Oxide/Photosensitive-Nanowire Composite Thin-Film Transistors for Transparent Multicolor Photodetectors Array. *Adv. Mater.* **2014,** *26*, 2919-2924.
(23) Tian, W.; Zhai, T.; Zhang, C.; Li, S.-L.; Wang, X.; Liu, F.; Liu, D.; Cai, X.; Tsukagoshi, K.; Golberg, D.; Bando, Y. Low-Cost Fully Transparent Ultraviolet Photodetectors Based on Electrospun ZnO-SnO_2 Heterojunction Nanofibers. *Adv. Mater.* **2013,** *25*, 4625-4630.
(24) Wang, J.; Yan, C.; Kang, W.; Lee, P. S. High-Efficiency Transfer of Percolating Nanowire Films for Stretchable and Transparent Photodetectors. *Nanoscale* **2014,** *6*, 10734-10739.
(25) Zhaoqiang, Z.; Tanmei, Z.; Jiandomg, Y.; Yi, Z.; Jiarui, X.; Guowei, Y. Flexible, Transparent and Ultra-Broadband Photodetector Based on Large-Area WSe_2 Film for Wearable Devices. *Nanotechnology* **2016,** *27*, 225501.
(26) Pawbake, A. S.; Waykar, R. G.; Late, D. J.; Jadkar, S. R. Highly Transparent Wafer-Scale Synthesis of Crystalline WS_2 Nanoparticle Thin Film for Photodetector and Humidity-Sensing Applications. *ACS Appl. Mater. Interfaces* **2016,** *8*, 3359-3365.
(27) Zheng, Z. Q.; Yao, J. D.; Yang, G. W. Growth of Centimeter-Scale High-Quality In_2Se_3 Films for Transparent, Flexible and High Performance Photodetectors. *J. Mater. Chem. C* **2016,** *4*, 8094-8103.
(28) Qu, Y.; Liao, L.; Li, Y.; Zhang, H.; Huang, Y.; Duan, X. Electrically Conductive and Optically Active Porous Silicon Nanowires. *Nano Lett.* **2009,** *9*, 4539-4543.
(29) Dai, Y.; Wang, X.; Peng, W.; Zou, H.; Yu, R.; Ding, Y.; Wu, C.; Wang, Z. L. Largely Improved Near-Infrared Silicon-Photosensing by the Piezo-phototronic Effect. *ACS Nano* **2017,** *11*, 7118-7125.

(30) Kim, J.; Lee, H.-C.; Kim, K.-H.; Hwang, M.-S.; Park, J.-S.; Lee, J. M.; So, J.-P.; Choi, J.-H.; Kwon, S.-H.; Barrelet, C. J.; Park, H.-G. Photon-Triggered Nanowire Transistors. *Nat. Nanotechnol.* **2017,** *12*, 963-968.

(31) Das, K.; Mukherjee, S.; Manna, S.; Ray, S. K.; Raychaudhuri, A. K. Single Si Nanowire (Diameter ≤ 100 nm) Based Polarization Sensitive Near-Infrared Photodetector with Ultra-High Responsivity. *Nanoscale* **2014,** *6*, 11232-11239.

(32) Rao, K. D. M.; Kulkarni, G. U. A Highly Crystalline Single Au Wire Network as a High Temperature Transparent Heater. *Nanoscale* **2014,** *6*, 5645-5651.

(33) Um, H.-D.; Kim, N.; Lee, K.; Hwang, I.; Hoon Seo, J.; Yu, Y. J.; Duane, P.; Wober, M.; Seo, K. Versatile Control of Metal-Assisted Chemical Etching for Vertical Silicon Microwire Arrays and their Photovoltaic Applications. *Sci. Rep.* **2015,** *5*, 11277.

(34) William, M.; Colm, G.; Hugh, G.; Gillian, C.; Justin, D. H.; Colm, O. D. Mesoporosity in Doped Silicon Nanowires from Metal Assisted Chemical Etching Monitored by Phonon Scattering. *Semicond. Sci. Technol.* **2016,** *31*, 014003.

(35) Chiappini, C.; Liu, X.; Fakhoury, J. R.; Ferrari, M. Biodegradable Porous Silicon Barcode Nanowires with Defined Geometry. *Adv. Funct. Mater.* **2010,** *20*, 2231-2239.

(36) Dai, G.; Zou, H.; Wang, X.; Zhou, Y.; Wang, P.; Ding, Y.; Zhang, Y.; Yang, J.; Wang, Z. L. Piezo-phototronic Effect Enhanced Responsivity of Photon Sensor Based on Composition-Tunable Ternary CdS_xSe_{1-x} Nanowires. *ACS Photonics* **2017,** *4*, 2495-2503.

(37) Zhou, J.; Huang, J. Photodetectors Based on Organic–Inorganic Hybrid Lead Halide Perovskites. *Adv. Sci.* **2017,** 1700256.

(38) García de Arquer, F. P.; Armin, A.; Meredith, P.; Sargent, E. H. Solution-Processed Semiconductors for Next-Generation Photodetectors. *Nat. Rev. Mater.* **2017,** *2*, 16100.

(39) Dou, L.; Yang, Y.; You, J.; Hong, Z.; Chang, W.-H.; Li, G.; Yang, Y. Solution-Processed Hybrid Perovskite Photodetectors with High Detectivity. *Nat. Commun.* **2014,** *5*, 5404.

(40) Gong, X.; Tong, M.; Xia, Y.; Cai, W.; Moon, J. S.; Cao, Y.; Yu, G.; Shieh, C.-L.; Nilsson, B.; Heeger, A. J. High-Detectivity Polymer Photodetectors with Spectral Response from 300 nm to 1450 nm. *Science* **2009,** *325*, 1665-1667.

(41) Kiruthika, S.; Singh, S.; Kulkarni, G. U. Large Area Transparent ZnO Photodetectors with Au Wire Network Electrodes. *RSC Adv.* **2016,** *6*, 44668-44672.

(42) Yang, S.; Tongay, S.; Yue, Q.; Li, Y.; Li, B.; Lu, F. High-Performance Few-Layer Mo-Doped $ReSe_2$ Nanosheet Photodetectors. *Sci. Rep.* **2014,** *4*, 5442.

(43) Xiang, D.; Han, C.; Zhang, J.; Chen, W. Gap States Assisted MoO_3 Nanobelt Photodetector with Wide Spectrum Response. *Sci. Rep.* **2014,** *4*, 4891.

(44) Liu, H.; Gao, N.; Liao, M.; Fang, X. Hexagonal-like Nb_2O_5 Nanoplates-Based Photodetectors and Photocatalyst with High Performances. *Sci. Rep.* **2015,** *5*, 7716.

(45) Kim, J.; Joo, S. S.; Lee, K. W.; Kim, J. H.; Shin, D. H.; Kim, S.; Choi, S.-H. Near-Ultraviolet-Sensitive Graphene/Porous Silicon Photodetectors. *ACS Appl. Mater. Interfaces* **2014,** *6*, 20880-20886.

(46) Ben-Chorin, M.; Möller, F.; Koch, F. Band Alignment and Carrier Injection at the Porous-Silicon–Crystalline-Silicon Interface. *J. Appl. Phys.* **1995,** *77*, 4482-4488.

(47) Wu, H.; Kong, D.; Ruan, Z.; Hsu, P.-C.; Wang, S.; Yu, Z.; Carney, T. J.; Hu, L.; Fan, S.; Cui, Y. A Transparent Electrode Based on a Metal Nanotrough Network. *Nat. Nanotechnol.* **2013,** *8*, 421-425.

(48) Sharma, A.; Bhattacharyya, B.; Srivastava, A. K.; Senguttuvan, T. D.; Husale, S. High Performance Broadband Photodetector Using Fabricated Nanowires of Bismuth Selenide. *Sci. Rep.* **2016,** *6*, 19138.

(49) Pao-Lo, L.; Williams, K. J.; Frankel, M. Y.; Esman, R. D. Saturation Characteristics of Fast Photodetectors. *IEEE Transactions on Microwave Theory and Techniques* **1999,** *47*, 1297-1303.
(50) Wu, J.; Zang, J.; Rathmell, A. R.; Zhao, X.; Wiley, B. J. Reversible Sliding in Networks of Nanowires. *Nano Lett.* **2013,** *13*, 2381-2386.
(51) Liu, H.; Pourret, A.; Guyot-Sionnest, P. Mott and Efros-Shklovskii Variable Range Hopping in CdSe Quantum Dots Films. *ACS Nano* **2010,** *4*, 5211-5216.
(52) Pichon, L.; Jacques, E.; Rogel, R.; Salaun, A. C.; Demami, F. Variable Range Hopping Conduction in N- and P-type *in situ* Doped Polycrystalline Silicon Nanowires. *Semicond. Sci. Technol.* **2013,** *28*, 025002.
(53) Park, J.; Lee, E.; Lee, K. W.; Lee, C. E. Electrical Transport and Quasipersistent Photocurrent in Vanadium Oxide Nanowire Networks. *Appl. Phys. Lett.* **2006,** *89*, 183114.
(54) González-Posada, F.; Songmuang, R.; Den Hertog, M.; Monroy, E. Room-Temperature Photodetection Dynamics of Single GaN Nanowires. *Nano Lett.* **2012,** *12*, 172-176.
(55) Ghosh, S.; Winchester, A.; Muchharla, B.; Wasala, M.; Feng, S.; Elias, A. L.; Krishna, M. B. M.; Harada, T.; Chin, C.; Dani, K.; Kar, S.; Terrones, M.; Talapatra, S. Ultrafast Intrinsic Photoresponse and Direct Evidence of Sub-gap States in Liquid Phase Exfoliated MoS_2 Thin Films. *Sci. Rep.* **2015,** *5*, 11272.

Graphical Table of Content:

Transparent, flexible Silicon nanostructured network for high performance broadband photodectors